Supplementary

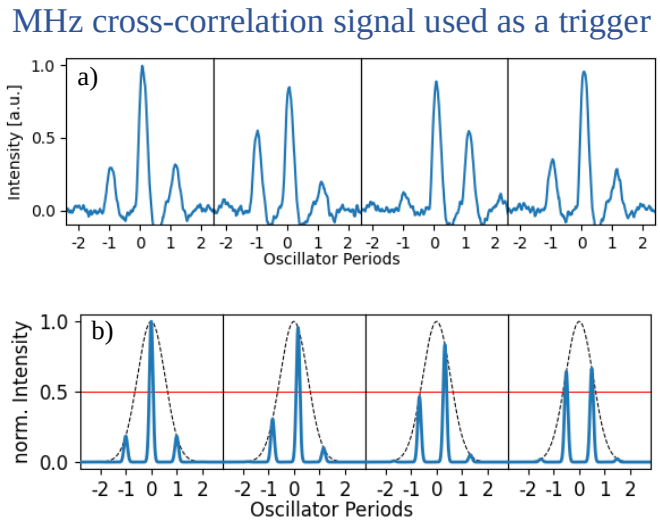

Figure S1: Oscillator output cross correlation (MHz-X): a) recorded, b) calculated showing the SFG envelope and trigger level

Fig. S1 shows the structure of the cross-correlation signal (measured and calculated) used to trigger the timing generators, where a fixed voltage level is used as the decision for the trigger event. Since we use fast photodiode and electronics, the individual SFG pulses can be resolved. These pulses lie underneath an envelope (dashed line) whose width is governed by the ratio between the time step and the pulse duration. Because the individual oscillator repetition rates are not an integer multiple of the repetition rate difference, the relative timing between the SFG pulses and the envelope is not fixed, and varies from one RA cycle to the next. Hence, the exact arrival time of the picked pulses fluctuates within the range of one delay step $\Delta t = 80$ fs for the case of 500 Hz repetition rate difference. The delay distribution in Fig. 4c of the main text, indicates that most jitter is introduced by the trigger uncertainty and that the added jitter from intensity noise, the amplifier cavities and beam path are low.

Regenerative Amplifiers:

The regenerative amplifiers (RA) used in this demonstration use the chirped pulse amplification technique to produce output pulses with smaller than 250 fs pulse duration and pulse energies up to 1 mJ at 1030 nm. We use a common stretcher where both oscillator channels pass with a small offset next to each other. Pulses are stretched to around 200 ps. To mitigate gain narrowing, a spectral shaper based on a single birefringent crystal followed by a thin-film polarizer (TFP) is used before amplification. For compression high efficiency transmission diffraction gratings (Gitterwerk) are used. To compress both channels on a single grating the compressor layout is mirrored around the grating plane. The first channel has its first bounce on the grating on the front-left while the second channel hits the back-right first. The second order dispersion can be controlled individually for both channels. Third order dispersion can be controlled by rotating the grating for both channels simultaneously and fine-tuned by adjusting the input angle of an individual channel.

Both amplifier cavities are built in a single monolithic encasing. Both cavities are placed mirrored around a common pump diode (nLight Pearl P16, 130W, 976nm). The pump diode is constructed from two stacks of 8 emitters. The stacks are collimated together and then geometrically split to the cavities on the right and left. The cavities follow a standard regenerative amplifier layout. Faraday rotators separate the in- and out-going pulses. β-barium borate (BBO) Pockels Cells with 4mm free apertures act as electro-optical switches. The timing for the Pockels Cells is set so that only a single oscillator pulse is locked into the cavity and amplified. The gain medium is ytterbium calcium fluoride

($Yb:CaF_2$) at room temperature. The mode size allows the operation of the amplifiers at 1 mJ pulse energy after the compressor in each channel.

As both the oscillator and amplifiers are built with the same gain medium ($Yb:CaF_2$), they operate at different population inversion levels, and hence the optimal operating regime of the amplifier (center wavelength 1030 nm with a FWHM bandwidth of 15 nm) is blue shifted with respect to the oscillator (center wavelength 1050 nm with bandwidth of 8 nm). As the whole amplification system, including stretcher and compressor, was built and designed for operation at 1030 nm the performance at 1050 nm was reduced in terms of spectral bandwidth and pulse duration. With seed at 1050 nm a FWHM bandwidth of 8 nm and pulse durations of around 600 fs were achieved.

Cross Correlation of the amplified femtosecond pulses in free-running mode:

When running the amplifiers not synchronized to the oscillator detuning (Δf_{rep}) pulses with increasing delay values are generated in an ASOPS style manner. Due to the mismatch between the regenerative amplifier repetition rate (f_{RA}) and the oscillator detuning (Δf_{rep}), the interpulse delay within the pair of amplified pulses is automatically incremented by $1/\Delta f_{rep}$, when $f_{RA} \sim \Delta f_{rep}$, with each amplifier shot and then wrapped around when the maximum sweep range, corresponding to the roundtrip of the oscillator cavity, is reached.

Figure S2 shows the output signal of the amplifiers (CH1 and CH2) as well as the recorded sum-frequency cross-correlation signal. The signals were recorded simultaneously, shot by shot, using an oscilloscope with 3 photodiodes, while triggering from CH2. The plots clearly show how CH1 scans a full oscillator roundtrip before wrapping around.

The data shown in this panel were recorded using two Yb:KGW oscillators (Flint, Light Conversion) with active stabilization. The oscillators were operated at 75.5 MHz with a detuning of ~ 10 kHz resulting in a step size of $\Delta t \sim 1.8$ ps for this demonstration.

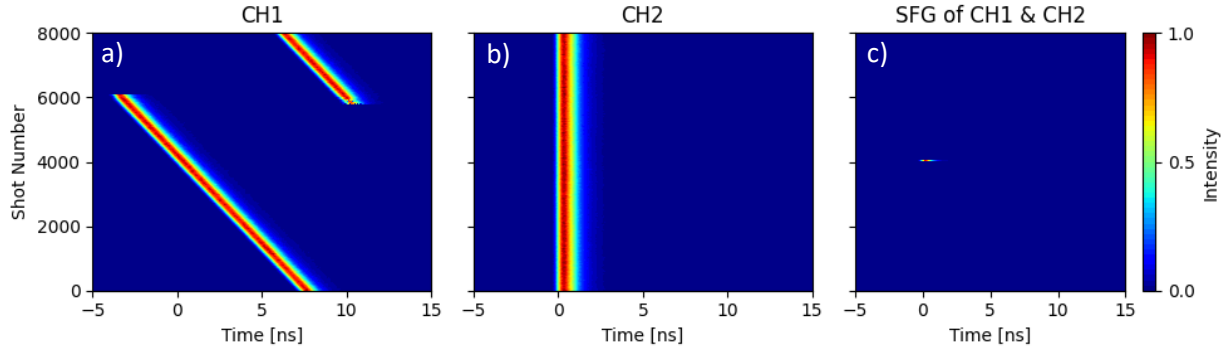

Figure S2: Cross-Correlation showing the signals for the two output channels (Panels a and b) and the sum-frequency cross-correlation signal (Panel c)

Active Stabilization

For preliminary measurements, we implemented a synchronization scheme for two solid-state Yb:KGW oscillators (Flint, Light Conversion), similar to the scheme reported by Gebs *et. al.* [1]. Due to limited availability of components, we settled for operating the phase-frequency detector at the 12th harmonic (~906 MHz) of the fundamental oscillator repetition rate instead of using harmonics around ~ 8 GHz as would be necessary to stabilize the repetition rate with femtosecond precision. Therefore, our stabilization loop was drifting in the order of several picoseconds and couldn't be used for the data shown in the manuscript. Nevertheless, it helped us in developing the trigger scheme for the regenerative amplifiers.

Description of the Polycrystalline thin film of $CH_3NH_3PbI_3$

For the pump-probe data a polycrystalline thin film of $CH_3NH_3PbI_3$ was used as a sample. This perovskite exhibits transient kinetics over multiple timescales. The ultrafast photophysics of $CH_3NH_3PbI_3$ was studied in detail before [2]. Briefly, immediately after light absorption, a non-thermal distribution of carriers is generated, and a Fermi-Dirac

distribution is formed through carrier-carrier scattering on timescales from a few to tens of femtoseconds, which our experiments are not aimed at resolving [2]. After this thermalization step, the distribution of carriers is left at a temperature higher than the lattice, and it cools down through electron-phonon scattering [3]. In transient absorption, the hot distribution of excitons is manifested in the form of two spectral signatures, displayed in Figure S3. The first is a photobleach tail on the blue side of the main exciton bleach, corresponding to bleach and stimulated emission from carriers with excess energy above the gap, and the second is a photoinduced absorption peak towards the red of the main exciton, due to a bandgap renormalization induced by the presence of hot carriers. As carriers cool down, both features disappear synchronously with a timescale of around 200 fs at low excitation densities ($<5\times10^{17}$ cm^{-1}), while at higher excitation densities a hot phonon bottleneck can substantially slow cooling timescales, reaching over tens of picoseconds [4, 5].

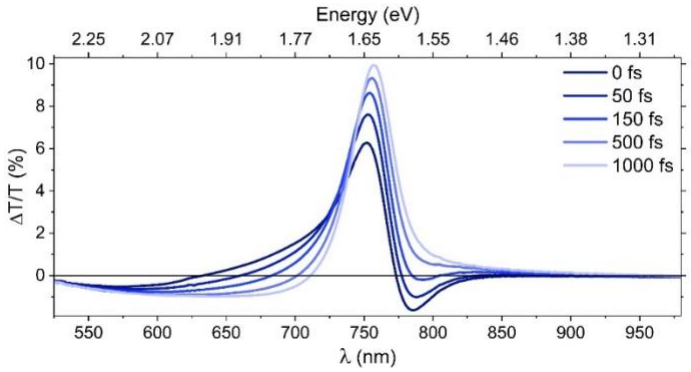

Figure S3: Transient absorption spectra of $CH_3NH_3PbI_3$ at different pump-probe delay times following photoexcitation at 620 nm [4].

References

1. R. Gebs, G. Klatt, C. Janke, T. Dekorsy, and A. Bartels, "High-speed asynchronous optical sampling with sub-50fs time resolution," Opt. Express 18, 5974-5983 (2010)
2. Richter, J. M.; Branchi, F.; Camargo, F. V. A.; Zhao, B.; Friend, R. H.; Cerullo, G.; Deschler, F. Ultrafast Carrier Thermalization in Lead Iodide Perovskite Probed with Two-Dimensional Electronic Spectroscopy. Nat. Commun. 2017, 8, 376. https://doi.org/10.1038/s41467-017-00546-z.
3. Ghosh, T.; Aharon, S.; Etgar, L.; Ruhman, S. Free Carrier Emergence and Onset of Electron-Phonon Coupling in Methylammonium Lead Halide Perovskite Films. J. Am. Chem. Soc. 2017, 139 (50), 18262–18270. https://doi.org/10.1021/jacs.7b09508.
4. Price, M. B.; Butkus, J.; Jellicoe, T. C.; Sadhanala, A.; Briane, A.; Halpert, J. E.; Broch, K.; Hodgkiss, J. M.; Friend, R. H.; Deschler, F. Hot-Carrier Cooling and Photoinduced Refractive Index Changes in Organic–Inorganic Lead Halide Perovskites. Nat. Commun. 2015, 6 (May), 8420. https://doi.org/10.1038/ncomms9420.
5. Yang, Y.; Ostrowski, D. P.; France, R. M.; Zhu, K.; van de Lagemaat, J.; Luther, J. M.; Beard, M. C. Observation of a Hot-Phonon Bottleneck in Lead-Iodide Perovskites. Nat. Photonics 2016, 10 (January), 53–59. https://doi.org/10.1038/nphoton.2015.213.